# Multi-Domain Modeling and Simulation of High Temperature Superconducting Transmission Lines under Short Circuit Fault Conditions

Meaghan Podlaski, *Student Member, IEEE*, Luigi Vanfretti, *Senior Member, IEEE*, Abhijit Khare, *Member, IEEE*, Mike Sumption, and Phillip Ansell

***Abstract*—Emission reduction in transportation requires advancements in aviation technologies enabling fully electrified propulsion, among which, the use of superconducting technologies can provide untapped benefits given their low weight and minimal losses for high-power transmission. However, to enable their use in aircraft electrical power systems additional considerations for electrical and thermal performance during faults is required in order to meet stringent aircraft safety requirements. In this work, a cryogenically cooled electric aircraft power system is studied under short circuit conditions for different cooling media. This system consists of a fuel cell, high temperature superconducting (HTS) transmission line, inverter, and motor, where each of their fault models have been explored. A trade-off study of the impedance of the fuel cell is conducted to identify the values at which the superconducting cable remains thermally stable after a short circuit fault, as it is crucial that the cable does not experience a thermal runaway.**

***Index Terms*—Electrified aircraft modeling, liquid hydrogen, fault analysis, cryogenic cooling, superconducting lines**

## I. Nomenclature

| | |
|---|---|
| CHEETA | Center for High-Efficiency Electrical Technologies for Aircraft |
| HTS | High temperature superconductor |
| PEM | Proton exchange membrane |

## II. Introduction

### A. Motivation

INCREASED demand for environmentally-friendly and economical transportation has led to the active exploration of electrified aircraft concepts. Of all of the methods of conventional transportation, however, commercial aircraft features power requirements typically far higher than equivalently-sized ground, marine, and rail systems. To produce electrified propulsion systems capable of meeting these high power requirements in a compact and high-efficiency fashion, we can usefully turn to the use of cryogenically-cooled superconducting materials. However, creating physical prototypes for these kinds of complex systems can be costly and difficult, indicating the important role that modeling and simulation have towards understanding the operation of these new concepts and associated responses to fault modes.

This research specifically focuses on the development of models and their application in simulation-based studies for the design of an electrified aircraft power system enabled by cryogenically cooled high temperature superconducting (HTS) transmission lines. There are two aspects that need to be captured: the electrical behavior and the thermal behavior, so system design, integration, and analysis can be performed for electrical and thermal management. To this end, to perform both the electrical and thermal designs together, we will need to use a technology and modeling methodology that allows us to combine both behaviors in an entire system model. Multi-domain models were created to capture each physical aspect of the power system, specifically the electrical and thermal domains of the HTS line; each component in the power system has an individual, reusable model based on the component's physical equations and behaviors. The models have been created using the object-oriented modeling language, Modelica. This paper introduces a model of HTS lines configured within a simple yet representative aircraft electrical power system, alongside the modeled response of the system operation to fault conditions. These results inform the design for the fully-electric aircraft concept currently under development by the Center for High-Efficiency Electrical Technologies for Aircraft (CHEETA).

### B. Related Works

Previous works have derived the mathematical models utilized in the current study and conducted experiments using liquid hydrogen ($LH_2$) to derive thermal response characteristics of the line [1], [2]. The electrical power systems subjected to the fault tests in this study were specified based on the CHEETA electrified aircraft system [3], and earlier models of the HTS lines and their application and integration with the CHEETA power system are described in [4].

HTS lines have been considered in electrified aircraft power system architectures due to the ability to carry high currents

This work was supported in whole or in part by the National Aeronautics and Space Administration under award number 80NSSC19M0125 as part of the Center for High-Efficiency Electrical Technologies for Aircraft (CHEETA), in part by the Engineering Research Center Program of the National Science Foundation and the Department of Energy under Award EEC-1041877 and the CURENT Industry Partnership Program, and by the Center of Excellence for NEOM Research at the King Abdullah University of Science and Technology under grant OSR-2019-CoE-NEOM-4178.12.

The first author is supported through the National Science Foundation Graduate Research Fellowship Program under Grant No. DGE 1744655 and Chateaubriand Fellowship Program.

M. Podlaski, L. Vanfretti, and A. Khare are with the Department of Electrical, Computer, and Systems Engineering, Rensselaer Polytechnic Institute, 110 8th St, Troy, NY 12180, USA. e-mail: {podlam, vanfrl, kharea}@rpi.edu.

M. Sumption is with the Department of Materials Science and Engineering, Ohio State University, 140 W 19th Ave, Columbus, OH 43210, USA. e-mail: sumption.3@osu.edu

P. Ansell is with the Department of Aerospace Engineering, University of Illinois Urbana-Champaign, 104 S Wright St, Urbana, IL, USA. e-mail: ansell1@illinois.edu

with low losses while not adding significant weight to the system. [5] proposes a temperature and time dependent thermo-electric model for an HTS cable according to the *E-J* power law. The failure modes focus on parameterizing the resistances and inductances of the line to mitigate different effects from the fault. In contrast, the HTS models described in this paper assume a fixed boundary condition between the thermal port of the cooling media and the cable, allowing for thermal behavior specific to the cooling media used in the model and in-depth system level analysis. Other studies on electric aircraft focus on conducting sensitivity studies adjusting the cable parameters [6] to prevent/observe the time it takes the line to quench. In our study, we focus on how the lumped electrical characteristics of other components in the power system need to be considered to prevent quenching altogether.

In land-based systems, fault studies have been conducted on HTS lines such as the one in [7]. The liquid nitrogen cooled HTS system in [7] is studied under utility fault conditions to analyze the current distribution of the line, where the studies primarily focus on the electrical behavior of the line instead of the thermal behavior with the objective of determining if both layers of the cable would quench under fault conditions. The land-based system in [8] presents a three-phase HTS cable operating at 110kV constructed for grid integration that is subject to various faults. The fault applied vary in severity (e.g. single phase short circuit, electrical insulation breakdown) with the goal of studying current distribution between phases and the shielding and conducting layers of the line. This is meant to aid in the design of protection systems in the electrical domain only. In contrast, for the CHEETA system fault study, the HTS line needs to be studied from at the system level to determine the effects of other components on the quenching of the line under fault conditions under consideration of both the electrical and thermal domains.

The thermal characteristics of the HTS line models are modeled with the equations in [9], and the treatment of heat transfer for the liquid nitrogen studied is derived from the experiments conducted in [2].

The HTS transmission line simulations of the present study also utilize cold-end cooling models based on studies in [9], which focuses on the detailed analysis of a ReBCO Roebel cable quench and stability. Reference [9] outlined the equations required to model an HTS line cooled in a liquid cooling bath for external and locally applied disturbances.

The heat transfer characteristics for a saturated liquid hydrogen cooling bath are determined from [1]. That paper studied heat transfer from a horizontal wire immersed in liquid and super-critical hydrogen for a wide range of bath temperatures and pressures.

In this work, the thermo-electrical response of an HTS cable placed within a representative electric aircraft power system is studied during fault conditions. Reference [3] outlines the power system, which consists of a fuel cell, the HTS line, and the powertrain. The powertrain is divided into three physical components: an inverter, a cryogenically cooled electrically excited synchronous machine, and a speed controller. The electrical dynamic model for the fuel cell is derived from [10], which provides the short circuit characteristics of proton exchange membrane (PEM) fuel cells.

The inverter requires a Thévenin equivalent model to conduct the fault analysis. Reference [11] provides such a model, where the common-mode behavior of the power electronics is provided in terms of a Thévenin common-mode equivalent circuit, which is reliable in predicting the worst-case behavior of the inverter. The Thévenin inverter modeling approach is also tested in [11] in a DC micro-grid system, which proves feasibility for using the equivalent model with the electric aircraft power system.

### C. Paper Contributions

This paper contributes the following:

- A multi-engineering domain (thermo-electrical) model for an HTS transmission line that has been corroborated against experimental cryogenic stablility studies. The thermal behavior of the HTS line has been studied for liquid and gas hydrogen and liquid nitrogen.
- An inter-operable and open source software implementation of the HTS model, using the open access and standardized Modelica language; facilitating reuse and research reproducibility.
- Fault analysis for a novel electrified aircraft electrical power system architecture that uses the proposed HTS line. These trade-off studies show how the unavoidable impedance of the fuel cell can actually be advantageous to the system design by using it to limit the quench current and temperature rise in the HTS cable to protect the cryogenic system after a short circuit.
- Thermal response analysis under different cooling media. These studies provide a comparison between the use of liquid hydrogen and gas hydrogen as coolant. The results show that liquid cooling offers substantial advantages over gas cooling for the thermo-electrical stability of the HTS line during faults.

### D. Paper Organization

This paper is organized as follows. In Section III, the physics- and equation-based models for the HTS line with both liquid and gas cooling are presented. The model is validated against previous experimental studies. In Section IV, the power system used for fault analysis studies is outlined. The model's response is analyzed for different cooling media in Section V. The results from the fault tests are discussed in Section VI.

## III. HTS Model

### A. Modelica and Multi-Domain Modeling Overview

Models used in the development of the HTS line for the CHEETA aircraft are created using the object-oriented equation-based modeling language, Modelica. The language provides inter-operability and model portability through an open access language specification [12], which is supported by different tools (see [13]). Modelica provides the flexibility to implement and interface models from different engineering domains by developing physically-meaningful equation-based interfaces between them. This means that the equations derived from the principles of physics and engineering are used to connect models together. The term 'domain' is used to denote a typical engineering area or discipline. In the case of the

HTS component, both electrical and mechanical domains are included in a singular model. All electrical variables are connected and modeled according to Ohm's Law, Kirchoff's Laws, and other electrical principles. Mechanical variables are modeled according to laws of kinematics, and the thermal variables obey the laws of thermodynamics. This approach enables modeling of the HTS line across multiple domains in an equation-based approach instead of having to reduce the model's Differential and Algebraic Equation System (DAES) into block-diagram oriented representations or declarative programming statements as done in other tools and languages.

Models created using Modelica can also be interchanged (i.e. using the `replaceable` keyword) by exploiting object-oriented programming principles to analyze models at varying levels of complexity, allowing users to analyze how different modeling assumptions affect system or component responses. This means models sharing the same `base class`, or same basic model outline, can be `replaceable` to one another. The HTS lines, for example, share the same `base class` of the electrical characteristics that can be made `replaceable` for different cooling mediums, facilitating model development, maintenance and re-use. This means one base model exists, but each cooling media has a specific heat transfer function. Such functions can be quickly exchanged to represent a cooling media without the need to change the entire model or to create multiple models for each kind of media. No model of the HTS line exists off-the-shelf for system level modeling, so it is necessary to integrate the functionalities for the thermal and electrical system.

The HTS line model described herein is studied under two cooling methods for three different cooling medias. The line is subject to liquid cooling using hydrogen and nitrogen as well as gas cooling using hydrogen gas. The comparison between liquid and gas cooling serves the purpose of showing that different cooling methods impact the sizing and weight of the cable, which is a significant constraint in the aircraft design. System level simulations for liquid nitrogen and liquid hydrogen cooled HTS lines allows for comparison between the sizing of a cable for each type of liquid cooling media.

### *B. CHEETA Electrical System One-Line Diagram*

The CHEETA electrical power system consists of energy sources (i.e. hydrogen fuel cells and batteries), power electronics (i.e. inverters), and other components that supply electrical power to motors that drive the fans for aircraft propulsion [3]. The CHEETA power system architecture is shown in Figure 1. Each group of fuel cells is connected via HTS transmission line to a distribution bus containing three machines, inverters, and a battery that is sized only to provide power only during transient flight conditions (e.g. fast maneuvers) due to weight/power density constraints. There are three branches for the electrical system, where they are connected at the fuel cell buses with a tie line for reliability.

All of the bus bars and transmission lines are encapsulated by a cryogenic environment, as designated by the blue lines of the system in Figure 1. The system is modeled to operate with each motor providing ≈1.6MW of power for a total cruise power of ≈14.4MW, with a rated power of 2.5 MW for high-

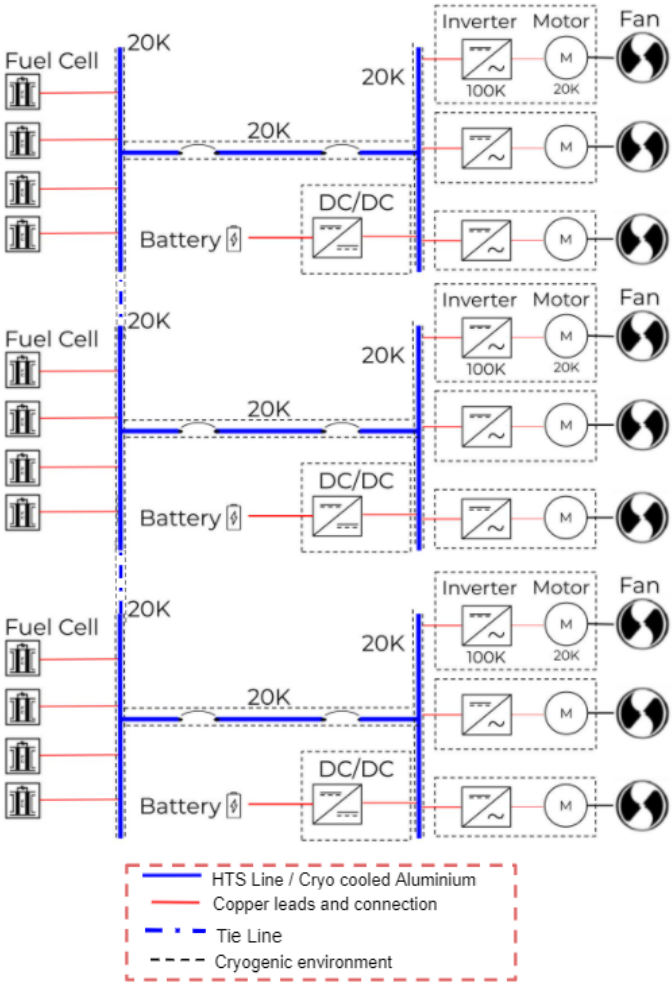


Fig. 1. The CHEETA electric aircraft architecture configured to show the electrical wiring scheme for the system. This schematic focuses on the electrical components; all cooling and thermal components are omitted. This representation only shows the go portion of the circuit, the return lines will also have the same structure.

power flight phases like takeoff and climb. Given the amount of time the aircraft spends in cruise, it is reasonable to suggest that a fault may be more probable under this flight phase. In conventional land-based electric power systems, normally the current in a system is minimized to limit the $I^2R$ losses on the line, resulting in an operating voltage that is considerably higher than the current. In the CHEETA aircraft concept, HTS components provide negligible losses when subject to cryogenic cooling, allowing for a system to operate at a much higher current and lower voltage. The HTS line is cooled separately at a temperature of 20-25 K from the rest of the cryogenic components. The transmission lines and bus bars are the components most vulnerable to failure due to uncontrollable heating, so it is crucial that the temperature is controlled in its own loop.

### *C. Model Overview: Liquid Cooled Transmission Line*

The HTS line is modeled using a co-axial cable electrical model with a thermal interface to model the cooling bath, which is shown in Figure 2. The blue blocks in the figure represent the electrical connections to external power system components such as the fuel cell and the inverter. The red box

is the thermal connection to the cooling bath, which couples the temperature and heat flow to the thermal behavior of the line. It should be noted that the inductive, capacitive, and most resistive components are time-varying, such that their values can change during a simulation depending on operational conditions as described below. In Figure 2, $R_L$ is the current lead resistance. $L_\pi$, $R_\pi$, and $C_\pi$ are the pi-line equivalent inductance, resistance, and capacitance, respectively. All variables, units, and definitions are listed in Appendix A.

The transmission line is modeled using the equations outlined in [14], [9]. The critical current $I_c$ is calculated by Equation 1, where it is a function of the temperature at the line surface $T$ and the transition temperature of the superconductor $T_c$. The electric field is calculated by Equation 2 as a function of the current through the transmission line $I_{op}$, the index value of the line $n$, the reference electric field $E_0$, and the critical current $I_c$. The resistivity of the line is calculated by Equation 3, where $A_{cu}$ is the cross sectional area of the tape in the line as projected onto a surface perpendicular to the line. For this line, the transition temperature ($T_c$) is 92 K, the reference electric field ($E_0$) is 1e-6 V/m, and the critical current at 20 K ($I_{c0}$) is 3700A.

$$I_c = I_{c0}(1 - \frac{T}{T_c}) \tag{1}$$

$$E = E_0 \left(\frac{I_{op}}{I_c}\right)^n \tag{2}$$

$$\rho = \frac{E \times A_{cu}}{I_{op}} \tag{3}$$

Equations 1, 2, and 3 are then used to calculate the values of the pi-line electrical model. In these equations we assume completely non-magnetic materials, so $\mu = \mu_0$ is the permeability of free space and $\epsilon = \epsilon_0$ is the dielectric permittivity. Equations 4, 5, and 6 determine the resistance, inductance, and capacitance of the line, respectively. In Equations 5 and 6, the values are dependent on the geometry of the cable, where $a$ is the inner radius of the co-axial cable and $b$ is the outer radius of the co-axial cable.

$$R_\pi = E_0 * \frac{\left(\frac{I_{op}}{I_c}\right)^n}{I_{op}} \qquad \Omega \text{ /m} \tag{4}$$

$$L_\pi = \frac{\mu}{2\pi} \log\left(\frac{b}{a}\right) \qquad \text{H/m} \tag{5}$$

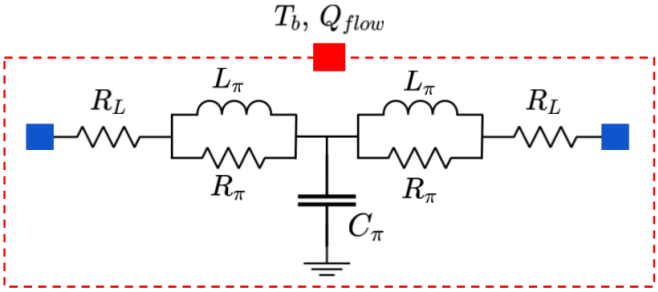


Fig. 2. HTS pi-line model schematic. When the line is modeled using Modelica, it is a multi-domain model consisting of thermal and electrical behavior as all electrical components are temperature dependent.

$$C_\pi = \frac{2\pi * \epsilon}{\log\left(\frac{b}{a}\right)} \qquad \text{F/m} \tag{6}$$

Equation 8 gives the $\Delta T_\rho$ for a given heat experienced by the cable; here there are two terms: the internally generated ohmic heat present during a quench and a potential perturbation $G_d$. The heat flow from the transmission line into the cooling bath is calculated by Equation 9. It is a function of the heat transfer coefficient ($h$), change in temperature ($\Delta T_\rho$), and cold-end cooling ($Q_{ce}$). The cold-end cooling excess heat flow is calculated using Equation 10. The heat transfer coefficient of liquid hydrogen is defined in Equation 7.

$$h = \begin{cases} 100(\Delta T_\rho)^{5.3} & \Delta T_\rho < 3 \\ \frac{10^5}{\Delta T_\rho} & 3 \leq \Delta T_\rho < 100 \\ 1000 & \Delta T_\rho \geq 100 \end{cases} \tag{7}$$

$$\Delta T_\rho = \frac{\left(\frac{\rho I_c^2}{P \times A_{cu}} + G_d\right)}{h} \tag{8}$$

$$Q_{flow} = h \times \Delta T_\rho + Q_{ce} \tag{9}$$

$$Q_{ce} = T_b \sqrt{2\kappa \times A_{cu} \times P \times h} \tag{10}$$

The equations above are necessary in order to study the HTS line under fault and quench conditions. Potential fault conditions can often be the most demanding constraint on the cooling conditions [9].

### *D. Model Overview: Gas Cooled Transmission Line*

Alternatively, the HTS model can be configured to consider the thermal response for hydrogen gas cooling methods. The electrical analytical expressions for the model under these conditions do not change; they follow Equations 1 - 6.

When the line is submerged in a liquid hydrogen bath, the difference in temperature between the cable and the cooling media is consistent for all points on the line. Gas cooling causes the difference between line temperature and the cooling media vary as a function of the distance from the inlet of the transmission line. The change in temperature, $\Delta T_z$, along the line is defined by Equations 11 and 12. All other equations for calculating the heat transfer remain the same from the liquid cooling case; the $h$ value is vastly different between gas and liquid in functional form. This results in a lower heat transfer value, leading to much higher temperatures in the line. The total change in temperature is represented by $\Delta T_{total}$ in Equation 13.

$$< T(z) >= T_{inlet} + \frac{Q_{flow} \times z}{v \times C_{pv} \times 2 \times \pi \times (R_c - R_0)^2} \tag{11}$$

$$\Delta T_z = < T(z) > - T_{inlet} \tag{12}$$

$$\Delta T_{total} = \Delta T_z + \Delta T_\rho \tag{13}$$

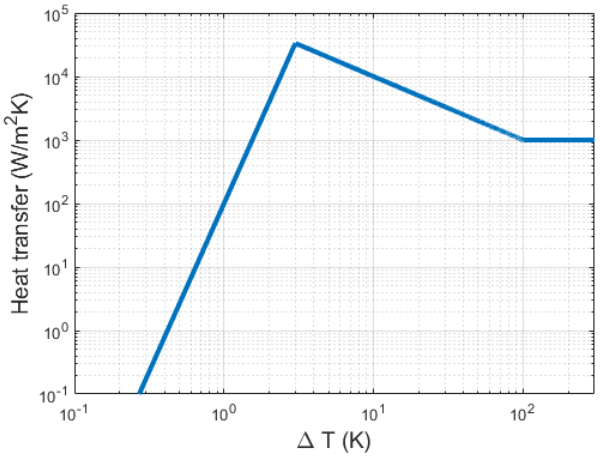


Fig. 3. Heat transfer characteristics as a function of temperature for the line submerged in a liquid hydrogen cooling bath.

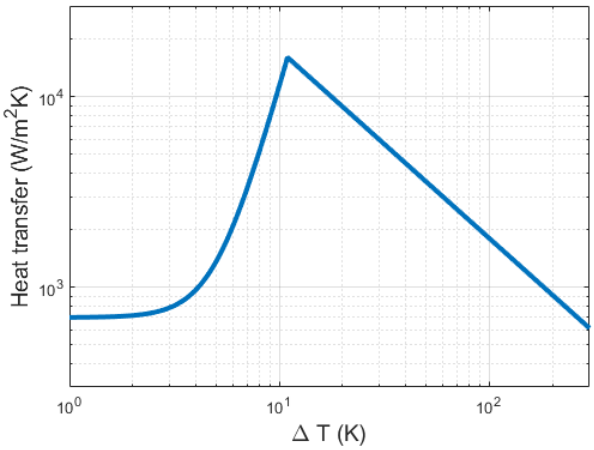


Fig. 4. Heat transfer characteristics as a function of temperature for the line submerged in a liquid nitrogen cooling bath.

## IV. Component Model Analysis

The physics defining the physical behavior of each individual domain used in the proposed HTS model has been corroborated against published results from previous studies such as [1], [2], and [9], where the component has been tested in isolation (i.e. with no other electric power system components) in laboratory experiments. Using the knowledge from these previous studies, i.e. recognizing that the physics and equations for the model fit an experimental real-world system, this work aims to assemble the electrical and thermal equations to implement the HTS model in an aircraft electrical power system with the purpose of design and analysis. Developing such model is valuable, as setting up an experiment of such kind would be costly to do for a system of this size, that does not exist and it is in early development phases. To this end, the work in [9] conducted by one of this paper's co-authors and the results from [1] were used to corroborate the equations and thermal behavior of the model, as illustrated in the results from this section. This ensures that the responses in the model are consistent with the responses and results in the literature so they can be used in system-level integration and analysis.

The HTS line system in Figure 6 is simulated to observe the V-I behavior of the line with the behavior outlined in [14] and [9]. To reproduce the behavior observed from laboratory experiments through the current set of simulations, a small voltage bias is applied to the line model. This means the voltage drops across the current lead resistance to produce a current in the line such that we can observe the desired V-I behavior. This is done to emulate how the experiment injected a current into the line; given that the present case has a very low load of only the current lead resistance, the associated required voltage is correspondingly low.

The heat transfer behavior of the line submerged in a liquid cooling bath is corroborated against the results from the literature in [1] as shown in Figure 3. The nucleate boiling regime occurs at $\Delta T_\rho$ below 3 K and the film boiling regime occurs at $\Delta T_\rho$ above 3 K. The heat transfer characteristics for nitrogen derived in [2], [9] are shown in Figure 4.

The HTS line is configured to be subject to gas cooling as shown in Figure 5. In this case, the current is swept

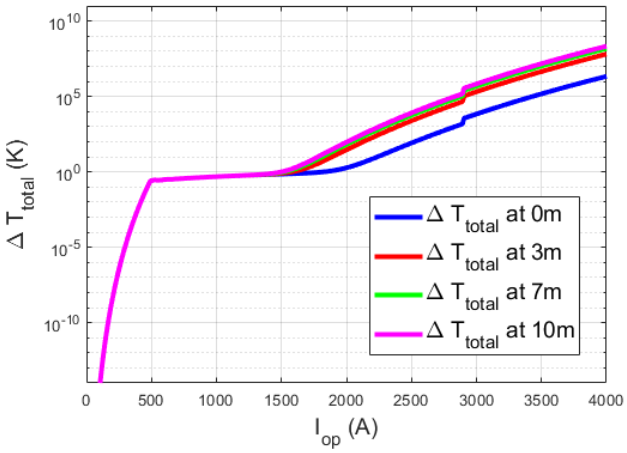


Fig. 5. Gas cooling $\Delta T_z$ vs $I_{op}$, where $\Delta T_z$ is the difference in temperature between the hydrogen gas and the cable at a distance (x) from the gas cooling inlet.

from 0 to 4kA, where the $I_{c0}$ of the line is 3.7kA. This is done with the goal of injecting a specific current into the line; the only load in the system is the current leads so the required voltage is also low. This shows that the severity of $\Delta T_z$ at shorter distances from the gas inlet increases as the current carried by the line approaches $I_c$. The observed change in $\Delta T_z$ drastically increases as compared to liquid hydrogen cooling $\Delta T_\rho$, especially at the end of the HTS line. This observation suggests that the gas cooling method presents reduced thermal stability and potential drawbacks for integration with the aircraft electrical power system.

## V. Fault Analysis

### A. Fault Model Overview

To illustrate the application of the HTS line model for aircraft electrical power system analysis, the HTS line model is integrated in a simplified yet representative version of the electrified aircraft electrical power system in [3]. The model consists of only one branch of the power system in [3], which is comprised of a fuel cell, an HTS line, an inverter, and an electrical motor operating as a load with a power factor of 0.91 lagging. The multi-domain system is shown in Figure 6, with

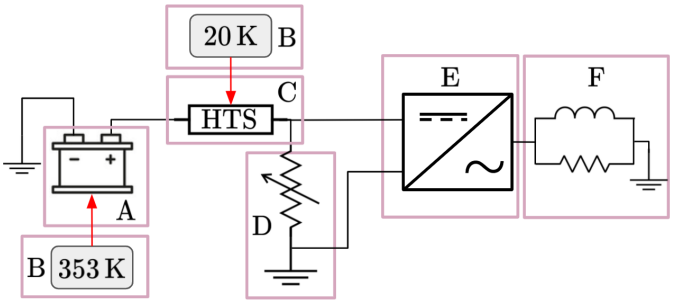


Fig. 6. Multi-domain aircraft electrical power system modeled using Modelica with each component used labeled.

both the HTS line and fuel cell modeled in both electrical and thermal domains. The components in the model are labeled as follows:

(A) PEM fuel cell (using model in Figure 7)
(B) Boundary conditions set by the cooling system for the fuel cell and HTS line, connected to thermal interface of the HTS line and fuel cell.
(C) HTS transmission line (using model in Figure 2)
(D) Fault resistance
(E) Inverter Thévenin equivalent (using model in Figure 8)
(F) Equivalent RL Load model representing the machine operating at a specified power factor

In this configuration, the ground is a reference voltage at 0 V. The schematic in Figure 6 only shows the "go" cable for the system; the return is implied. The return line in the system is at 0 V denoted as a common reference voltage. When there is a fault, we assume that the fault occurs between the go cable and the return cable fixed at 0 V.

The thermal interface with the inverter is omitted from the system because the Thévenin equivalent model does not allow for adequate modeling of the thermal behavior of the inverter. To properly model the thermal interface, the thermal impedance of the IGBT under the proposed cryogenic conditions is needed, which is not currently available. In future studies and development when such data becomes available, this behavior will be added as this will have an impact on the cooling media consumption and losses. Similarly, the regenerative capabilities are excluded from the model as the potential for regeneration will be limited by several factors: (a) the superconducting motor design, and (b) the ability to store/utilize re-generated energy. Finally, the CHEETA system design uses fuel cells as the main energy source for propulsion, the role of the batteries is limited to address transients due to weight constraints. Since the size of the batteries is limited due to their projected weight, which means that the potential for regeneration is trivial compared to the amount of energy used for propulsion [15].

*1) PEM Fuel Cell Model:* The fuel cell model is derived from the electrical circuit model for a PEM fuel cell in [10], [16] and is implemented using Modelica. The electrical circuit is shown in Figure 7. It consists of a cell voltage denoted as $E_{cell}$, multiple resistances and a capacitor, which values are defined by Equations 14, 15, and 16. Equations 14 and 15 are both temperature and current dependent components. The activation $R_{act}$ and concentration $R_{conc}$ resistances depend on the current generated by the fuel cell, $I_{FC}$, which is the operating current of the HTS line (used in Equations 2, 4) because they are connected in series. In Equations 14 and 15, which calculates the activation $R_{act}$ and concentration $R_{conc}$ resistances respectively, $R$ is the universal gas constant, $T_f$ is the temperature of the fuel cell, $I_{FC}$ is the fuel cell current, $\alpha$ is the electron transfer coefficient, $F$ is the Faraday constant, $n_e$ is the number of electrons, and $I_{max}$ is the maximum fuel cell current.

$$R_{act} = -\frac{RT_f \ln(I_{FC})}{\alpha n_e F I_{FC}} = \frac{V_{act,2}}{I_{FC}} \tag{14}$$

$$R_{conc} = -\frac{RT_f}{n_e F I_{FC}} \ln\left(\frac{-I_{FC}}{I_{max}}\right) \tag{15}$$

Equation 16 is the resistance of the polymer membrane ($R_{ohm}$), which consists of the resistance in between the membrane and electrodes, and the resistances of the electrodes [16]. $R_{ohm0}$ is the constant portion of $R_{ohm}$, $k_{RI}$ is an empirical constant for calculating $R_{ohm}$ as a function of current, and $k_{RT}$ is an empirical constant for calculating $R_{ohm}$ as a function of temperature. This resistance is connected to the activation and concentration resistances in series as shown in Figure 7.

$$R_{ohm} = R_{ohm0} + k_{RI} I_{FC} - k_{RT} T_f \tag{16}$$

The output voltage of the fuel cell is calculated using Equation 17. The activation voltage, which is a voltage drop that is only affected by the fuel cell's internal temperature, is described empirically by the Tafel equation in Equation 18. In Equation 19, $\eta_0$ is the temperature invariant part of the activation voltage, which is measured in K. The terms $a_{FC}$ and $b_{FC}$ in Equations 19 and 20 is a constant term used in the Tafel equation. The voltage drop across the capacitor in Figure 7 can be determined using Equation 21.

$$V_{out} = E_{cell} - V_c - V_{ohm} - V_{act1} \tag{17}$$

$$V_{act} = \eta_0 + (T_f - 298)a_{FC} + T_f b_{FC} \ln(I_{FC}) \tag{18}$$

$$V_{act1} = \eta_0 + (T_f - 298)a_{FC} \tag{19}$$

$$V_{act2} = T_f b_{FC} \ln(I_{FC}) \tag{20}$$

$$V_C = (I_{FC} - C\frac{dV_C}{dt})(R_{act} + R_C) \tag{21}$$

The fuel cell has a power capacity of 2.5MW and is parameterized with the stack values for the SR-12 stack from [16]. It operates at 1000V.

*2) Inverter Model:* The inverter model used in the fault analysis circuit is an averaged model reduced to a Thèvenin equivalent, which is derived from the model outlined in [11]. The purpose for using this model is because the common-mode behavior of the converter must be modeled to analyze the circuit and predict the worst-case common-mode response. Hence, the Thévenin equivalent model satisfied the needs for the fault analysis studies herein. The electrical model is shown in Figure 8.

The Thévenin impedance is calculated using Equation 22, which is a function of the common mode resistance, $R_{cm}$, and

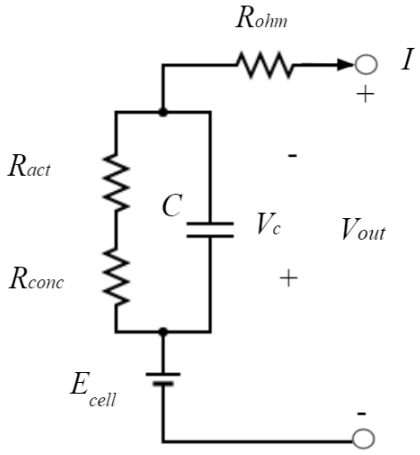


Fig. 7. PEM fuel cell electrical circuit diagram.

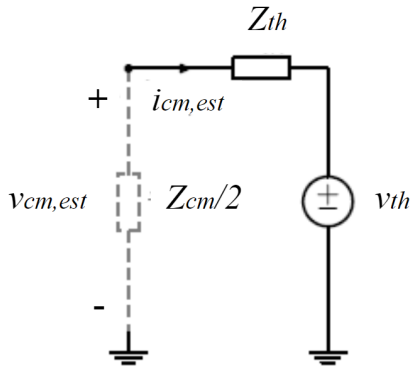


Fig. 8. Thevenin equivalent electrical model for common-mode operation of inverter [11].

diode resistance, $R_D$. The Thévenin voltage is determined by Equation 23, which is a function of the common mode voltage.

$$Z_{th} = \frac{R_D}{3} + R_{cm} \tag{22}$$

$$V_{th} = \frac{v_{cm,est}}{2} \tag{23}$$

### B. Fault Studies

The fault studies conducted below use the circuit shown in Figure 6. To simulate fault conditions, at the beginning of the simulation period, the fault's variable resistor in block D (see Figure 6) is set to 1 MΩ to limit current draw, and then drops to $\approx 0\Omega$ when the fault is applied, thereby creating a bolted fault. The line is given a critical current carrying capacity $I_{c0}$ of 3700 A, which translates to critical current $I_c$ of 2870 A at 20 K.

In addition, a trade-off analysis is conducted by performing a parametric sweep total fuel cell impedance in Figure 7, allowing the electro-thermal stability boundary of the aggregate source impedance to be determined. For impedance above this threshold the HTS line remains stable after the fault event. However, for impedance values lower than this threshold, the system experiences a quench event, characterized by an uncontrollable heating of the HTS line after a fault occurs.

Finally, the studies analyze different types of cooling media and methods in order to determine which method will offer the best fault performance. The types of media analyzed are hydrogen and nitrogen. For the case of hydrogen, both liquid and gas cooling are analyzed. These results are needed to provide requirements to the cooling system design, which will be addressed in future work.

*1) Liquid Hydrogen Cooling:* The HTS line is cooled with liquid hydrogen for the power system model shown in Figure 6. The equivalent resistance of the PEM fuel cell system in Figure 7 is swept over 20 values to determine the fuel cell impedance that best serves to protect the HTS system from quenching. The heat transfer of the HTS line follows the behavior in Figure 3.

The change in temperature prior to applying the short circuit as a function of the fuel cell impedance is shown in Figure 9. When the resistance of the fuel cell is zero, $\Delta T_\rho$ is 1.63 K. This ensures that the line will stay below the film boiling region when operating in steady state with the expected load. When the line is cooled with liquid hydrogen, the line can operate at approximately 2.43 times the critical current $I_c$ before entering film boiling. After the short circuit fault is applied, the change in line temperature is modeled to rise to an exceedingly high temperature, indicating a thermal failure of the HTS material. Figure 10 shows that the line will rise to an unstable temperature for any fuel cell equivalent resistance value below 0.414 Ω, which for resistance above this, we ensure that the line will remain below film boiling after the short circuit. This trend is observed due to the HTS line quenching whenever the change in temperature ($\Delta T_\rho$) is above 3 K, which is based on the heat transfer characteristics of the line in Figure 3.

*2) Liquid Nitrogen Cooling:* A similar study was also conducted with the HTS line thermal behaviors replaced with the liquid nitrogen heat transfer characteristics (shown in Figure 4). The nitrogen-cooled line is stable when the change in temperature ($\Delta T_\rho$) is below 11 K. The line's thermal behavior and carrying current prior to applying the short circuit fault is shown in Figure 11. When the $R_{ohm} \approx 0$, $\Delta T_\rho$ is exceedingly high, making the line thermally unstable and indicating a failure of the HTS material. The equivalent fuel cell resistance must be at least 0.345 Ω for the line to be cryogenically stable in normal operation conditions. In addition, it should be noted that the nitrogen cooled line does not offer the same safety factor as liquid hydrogen before the cooling media enters the film boiling region. This means that the liquid hydrogen will remain in the cryogenic regime for a carrying current of approximately twice the rated current capacity. In liquid nitrogen cooled cases, the line stays thermally stable only for operational currents less than the rated maximum capacity; the line will not remain in the cryogenic regime if this is exceeded unlike the liquid hydrogen case.

The same sweep of the fuel cell impedance is applied as in the liquid hydrogen case. Figure 12 shows that the line is thermally stable for fuel cell impedance larger than 0.548 Ω when a short circuit fault is applied at the inverter terminals.

*3) Hydrogen Gas Cooling:* Simulations were also conducted with the line's heat transfer characteristics set to represent the behavior of hydrogen gas. Hydrogen gas cooling is stable when the difference between the line temperature and gas is less than 3 K. Because hydrogen gas heats up as

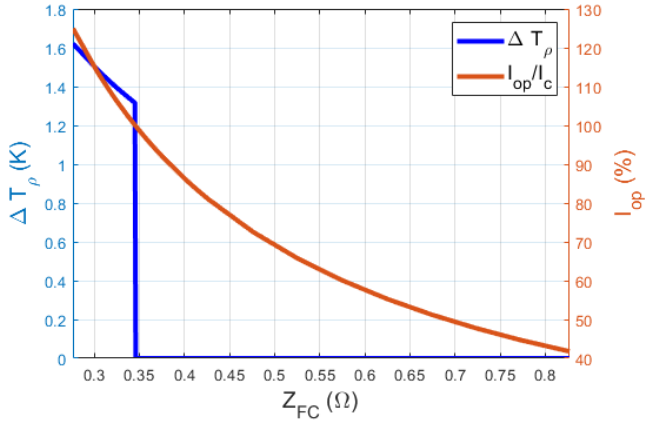


Fig. 9. Difference between in HTS line and cryogen temperature ($\Delta T_\rho$) and fraction of operational current (Iop) as a function of fuel cell impedance prior to applying the short circuit fault in **liquid hydrogen** cooling media.

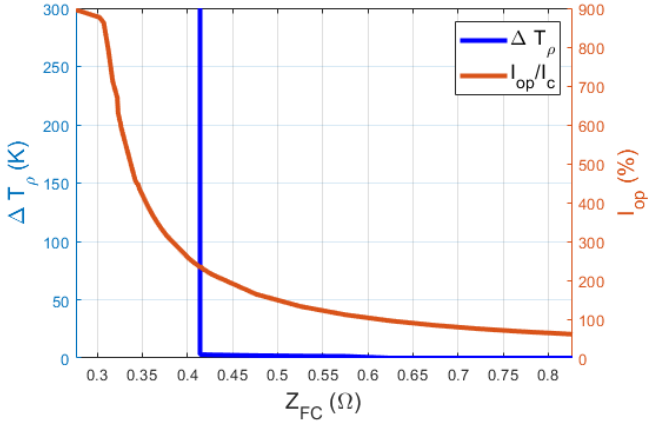


Fig. 10. Difference between in HTS line and cryogen temperature ($\Delta T_\rho$) and fraction of operational current (Iop) as a function of fuel cell impedance after to applying the short circuit fault in **liquid hydrogen** cooling media.

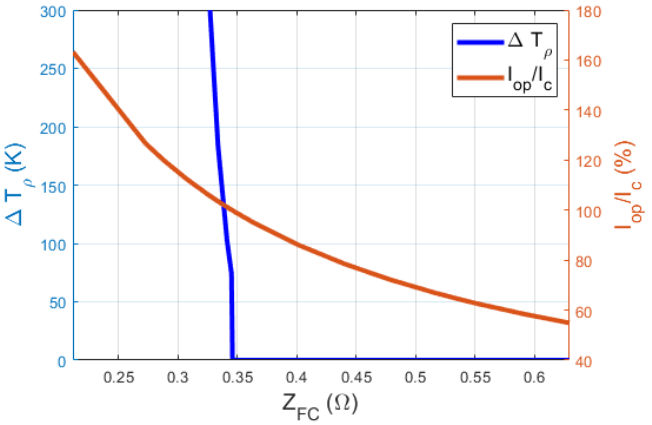


Fig. 11. Difference between in HTS line and cryogen ($\Delta T_\rho$) and fraction of operational current (Iop) as a function of fuel cell impedance prior to applying the short circuit fault in **liquid nitrogen** cooling media.

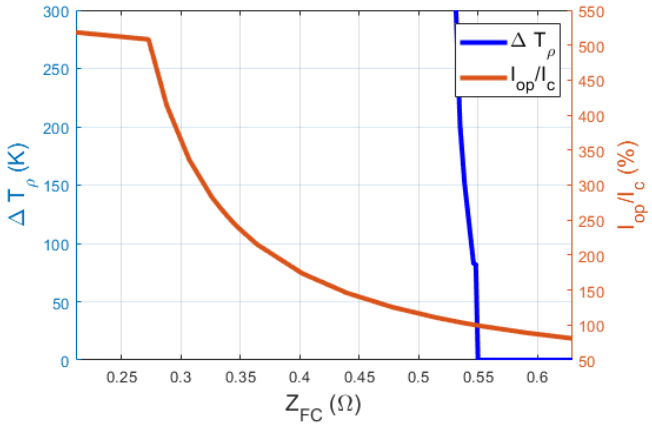


Fig. 12. Difference between in HTS line and cryogen ($\Delta T_\rho$) and fraction of operational current (Iop) as a function of fuel cell impedance after applying the short circuit fault in **liquid nitrogen** cooling media.

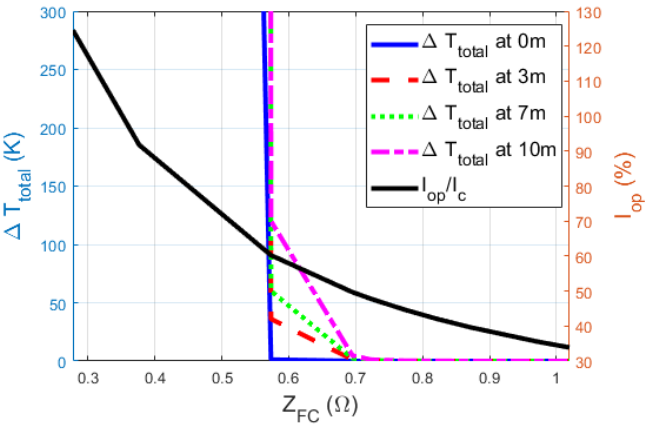


Fig. 13. Difference between in HTS line and cryogen ($\Delta T_z$) at different locations and fraction of operational current (Iop) as a function of fuel cell impedance prior to applying the short circuit fault in hydrogen gas cooling media.

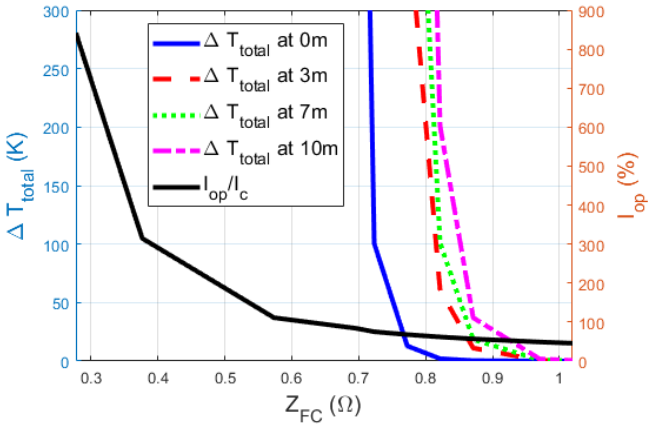


Fig. 14. Difference between in HTS line and cryogen ($\Delta T_z$) at different locations and fraction of operational current (Iop) as a function of fuel cell impedance after applying the short circuit fault in hydrogen gas cooling media.

a function of the distance from the inlet of the line cooling system, the HTS line's length as a function of the gas inlet's location must be carefully considered.

Figure 13 shows the change in line temperature as a function of the distance from the inlet of the hydrogen gas according to Equation 11. Hydrogen gas is not as effective at removing heat as liquid nitrogen or hydrogen. When the fuel cell impedance is 0.723 Ω, the temperature difference of the hydrogen gas from the inlet to the furthest point on the 10m line stays below the quench temperature prior to the short circuit. The line is operating at 49.6% of the maximum current capability, which limits the robustness of the HTS line and requires a significantly more robust cable design for the same current transfer in the liquid hydrogen and nitrogen cases.

When the short circuit is applied, the line is quenched for any fuel cell impedance below 0.871 Ω. This means that difference in temperature $\Delta T_z$ of the hydrogen gas from its inlet to the line and the measured temperature at every point in the line is less than 3 K. The line is operating at 56% of the maximum operational current for the line under these conditions. This implies that the line must be designed to have nearly four times the current capacity for the same line used with different cooling media.

## VI. Conclusion

An electric aircraft power system that uses HTS lines with cryogenic cooling has been modeled for fault analysis studies that help inform cooling design by considering different cooling methods and media. Using a multi-domain, thermo-electrical model of the HTS line within a simple yet representative aircraft system, fault simulations were conducted to inform different trade-offs in the power system electro-thermal design. It was observed that proper sizing of the fuel cell would need to take into account also the characterization of the aggregate equivalent impedance to protect the HTS line when there is a short circuit in the system, alongside observations of the cooling requirements that each media and method should meet to prevent a quench event. While the variable value of the fuel cell impedance itself cannot be controlled, it provides understanding of how the cable can be designed to be protected in both normal and fault conditions. The studies were conducted for three different cooling mediums: liquid hydrogen, liquid nitrogen, and hydrogen gas. When the transmission lines are submerged in liquid hydrogen, the line remains thermally stable for nearly twice the rated current. This behavior shows that liquid hydrogen cooling allows the system to operate safely and thermally stable under the worst fault conditions considered. This characteristic also provides a buffer to intermittent surge events in the line current, allowing the system to operate safely without having to implement any redundant lines or other protection equipment. This design approach minimizes HTS system size and weight, which is crucial for an aircraft's electrical power system.

Liquid hydrogen cooling provides an operational buffer before quench, where the line can carry currents up to twice the critical current prior to quench. When the lines are subject to cooling with liquid nitrogen and hydrogen gas, the system does not have this buffer and only stays stable when the system remains under the rated current. This gives inherent reliability to and allows for a smaller line to be used in the case of liquid hydrogen cooling, where other cooling methods require adjustment in the line sizing for fault protection. Since this HTS line will be used in an aircraft electrical power system, it is necessary to size the line so that it is as light as possible. The liquid hydrogen cooled HTS line quenches at a lower fuel cell impedance than the liquid nitrogen and hydrogen gas cooled cases, meaning that the line is more flexible for integration with various fuel cell designs and is a good candidate for lower impedance fuel cells. The drawback of gas cooling are that the line does not have the same buffer before quenching as compared to the liquid hydrogen or liquid nitrogen cooling would have for the same cable size. As a result, the gas cooled cable would need to be sized larger or multiple cables would need to be included in the electrical power system design to re-distribute the current. This would add weight to a system where minimizing weight is a priority.

Future work will expand the thermo-electrical modeling, by including models of cryogenically-cooled bus bars, and thermal modeling of other components in the system which have not included in this work (i.e. inverter and motor) to perform an integrated cooling system design that meets the specified boundary conditions in this paper during fault conditions. Other system configurations will also be considered in the future, including studying the system with a battery as a power source and cryogenic bus bars connecting the HTS line to the powertrain. The current leads will be modeled in further detail in the future to consider the dynamic effects of vapor cooling.

## Appendix A - Parameter Definitions

| Parameter | Description | Unit |
|---|---|---|
| | **HTS - Electrical Parameters** | |
| $C_\pi$ | Pi-Line Capacitance per unit length | F/m |
| $E_0$ | Reference electric field | V/m |
| $E$ | Electric field | V/m |
| $f$ | Frequency of AC system | Hz |
| $L_\pi$ | Pi-Line Inductance per unit length | H/m |
| n | Index value of superconductor | N/A |
| $I_{op}$ | Current into the HTS line | A |
| $I_{c0}$ | Critical current at 0 °K | A |
| $I_c$ | Critical current at 20 °K | A |
| $R_{AC}$ | Pi-Line AC Resistance | Ω |
| $R_L$ | Resistance of the brass connectors | Ω |
| $R_\pi$ | Pi-Line Resistance per unit length | Ω/m |
| $\omega$ | Frequency of AC system | rad/sec |
| $\tan\delta$ | Phase angle lag in AC operation | N/A |
| $\mu_r$ | Relative conductivity of wire material | N/A |
| $\epsilon_r$ | Relative permittivity of wire material | N/A |
| $\rho$ | Resistivity of HTS tape | $\Omega m$ |
| | **HTS - Thermal Parameters** | |
| $C_{pv}$ | Heat capacity of gas coolant | $J/K$ |
| $G_d$ | Energy perturbation causing a fault | $W/m^2$ |
| h | Heat transfer coefficient | $W/m^2K$ |
| $Q_{ce}$ | Cold-end cooling of the line | W |
| $Q_{flow}$ | Heat flow out of the line | W |
| $T_b$ | Cooling bath temperature | °K |
| $T_c$ | Critical temperature | °K |
| $T_{inlet}$ | Inlet temperature for gas cooling | °K |

| | | |
|---|---|---|
| $T(z)$ | Temperature of gas coolant as a function of linear distance | $^{\circ}$K |
| $v$ | Velocity of gas coolant | $m/s$ |
| $z$ | Distance from gas coolant inlet | $m$ |
| $\Delta T_{\rho}$ | Temperature jump at interface between cryogen and HTS surface | $^{\circ}$K |
| $\Delta T_{total}$ | Total temperature jump at interface between cryogen and HTS surface in gas cooling | $^{\circ}$K |
| $\Delta T_z$ | Temperature jump at interface between cryogen and HTS surface at a distance (z) from inlet of gas cooling | $^{\circ}$K |
| $\kappa$ | Cable thermal conductivity | $W/mK$ |
| | **HTS - Geometrical Parameters** | |
| $A_{cu}$ | Cross sectional area of copper portion of wire | $m^2$ |
| a | Inner radius of co-axial cable | $mm$ |
| b | Outer radius of co-axial cable | $mm$ |
| $P$ | Circumference of line | $m$ |
| $R_c$ | Inner radius of cryostat | $m$ |
| $R_0$ | Outer radius of cable | $m$ |
| | **Fuel Cell Parameters** | |
| $a_{FC}$ | Constant term in Tafel equation to calculate activation voltage | $V/K$ |
| $b_{FC}$ | Constant term in Tafel equation to calculate activation voltage | $V/K$ |
| $I_{FC}$ | Fuel cell current | A |
| $I_{max}$ | Fuel cell maximum current | A |
| $E_{cell}$ | Fuel cell internal voltage | V |
| $F$ | Faraday Constant | $A/mol$ |
| $k_E$ | Empirical constant to calculate $E_{cell}$ | V/K |
| $k_{RI}$ | Empirical constant to calculate $R_{ohm}$ | $\Omega/A$ |
| $k_{RT}$ | Empirical constant to calculate $R_{ohm}$ | $\Omega/K$ |
| $n_e$ | Number of electrons | N/A |
| $R$ | Universal gas constant | $J/mol$ |
| $R_{act}$ | Activation resistance | $\Omega$ |
| $R_{conc}$ | Concentration resistance | $\Omega$ |
| $R_{ohm}$ | Ohmic loss resistance | $\Omega$ |
| $R_{ohm0}$ | Reference term used in ohmic loss resistance calculation | $\Omega$ |
| $T_f$ | Temperature of fuel cell | $^{\circ}$K |
| $V_{out}$ | Output voltage of fuel cell | V |
| $V_c$ | Voltage drop from internal capacitance | V |
| $V_{ohm}$ | Voltage drop from ohmic loss, $R_{ohm}$ | V |
| $V_{act}$ | Total voltage drop from activation loss from $R_{act}$, $V_{act1} + V_{act2}$ | V |
| $V_{act1}$ | Voltage drop due to activation loss from $R_{act}$ only dependent on fuel cell internal temperature | V |
| $V_{act2}$ | Voltage drop due to activation loss from $R_{act}$ dependent on fuel cell internal temperature and current | V |
| $\alpha$ | Electron transfer coefficient | N/A |
| $\eta_0$ | Temperature invariant part of $V_{act}$ | V |
| | **Inverter Parameters** | |
| $R_{cm}$ | Common-mode resistance | $\Omega$ |
| $R_D$ | Diode resistance | $\Omega$ |
| $V_{cm,est}$ | Common-mode voltage | V |
| $V_{th}$ | Thevenin voltage | V |
| $Z_{th}$ | Thevenin impedance | $\Omega$ |

## REFERENCES


[1] H. Tatsumoto, Y. Shirai, M. Shiotsu, Y. Naruo, H. Kobayashi, and Y. Inatani, "Heat transfer characteristics of a horizontal wire in pools of liquid and supercritical hydrogen," *Journal of Superconductivity and Novel Magnetism*, vol. 28, 03 2014.

[2] M. Kida, Y. Kikuchci, O. Takahashi, and I. Michiyoshi, "Pool-boiling heat transfer in liquid nitrogen," *Journal of Nuclear Science and Technology*, vol. 18, no. 7, pp. 501–513, 1981. [Online]. Available: https://doi.org/10.1080/18811248.1981.9733284

[3] M. Podlaski, L. Vanfretti, H. Nademi, P. J. Ansell, K. S. Haran, and T. Balachandran, *Initial Steps in Modeling of CHEETA Hybrid Propulsion Aircraft Vehicle Power Systems using Modelica*. [Online]. Available: https://arc.aiaa.org/doi/abs/10.2514/6.2020-3580

[4] M. Podlaski, L. Vanfretti, A. Khare, M. Sumption, and P. J. Ansell, *Multi-Domain Modeling for High Temperature Superconducting Components for the CHEETA Hybrid Propulsion Power System*.

[5] S. S. Fetisov, V. V. Zubko, S. Y. Zanegin, A. A. Nosov, V. S. Vysotsky, A. Kario, A. Kling, W. Goldacker, A. Molodyk, A. Mankevich, V. Kalitka, A. Adamenkov, S. Samoilenkov, and D. Melyukov, "Development and characterization of a 2g hts roebel cable for aircraft power systems," *IEEE Transactions on Applied Superconductivity*, vol. 26, no. 3, pp. 1–4, 2016.

[6] K. M. Davies, P. J. Norman, C. E. Jones, S. J. Galloway, and G. M. Burt, "Fault behaviour of a superconducting turboelectric distributed propulsion aircraft network: A comprehensive sensitivity study," in *2015 International Conference on Electrical Systems for Aircraft, Railway, Ship Propulsion and Road Vehicles (ESARS)*, 2015, pp. 1–6.

[7] J.-H. Kim, M. Park, J. Cho, K. Sim, S. Kim, and I.-K. Yu, "Current distribution analysis of conducting and shield layers of hts power cable under utility fault condition," *IEEE Transactions on Applied Superconductivity*, vol. 19, no. 3, pp. 1718–1721, 2009.

[8] J. Li, Z. Zhao, B. Shu, X. Han, X. Ma, B. Bian, J. Li, and Z. Liang, "Fault analysis for 110 kv hts power cables," *IEEE Transactions on Applied Superconductivity*, vol. 24, no. 5, pp. 1–5, 2014.

[9] C. Kovacs, M. Majoros, M. Sumption, and E. Collings, "Quench and stability of roebel cables at 77k and self-field: Minimum quench power, cold end cooling, and cable cooling efficiency," *Cryogenics*, vol. 95, pp. 57 – 63, 2018. [Online]. Available: http://www.sciencedirect.com/science/article/pii/S0011227517304472

[10] F. Grumm, M. Schumann, C. Cosse, M. Plenz, A. Lücken, and D. Schulz, "Short circuit characteristics of pem fuel cells for grid integration applications," *Electronics*, vol. 9, p. 602, 04 2020.

[11] T. J. Donnelly, S. D. Pekarek, D. R. Fudge, and N. Zarate, "Thévenin equivalent circuits for modeling common-mode behavior in power electronic systems," *IEEE Open Access Journal of Power and Energy*, vol. 7, pp. 163–172, 2020.

[12] Modelica Association, "Modelica Language Specification," Online, February 2021, version 3.6-dev. [Online]. Available: https://github.com/modelica/ModelicaSpecification

[13] M. Association, "Modelica Tools," Online, September 2021. [Online]. Available: https://modelica.org/tools

[14] Z.J.J Stekly and J.L. Zar, "Stable superconducting coils," *IEEE Transactions on Nuclear Science*, vol. 95, pp. 367–372, 06 1965.

[15] E. Waddington, J. M. Merret, and P. J. Ansell, *Impact of LH¡sub¿2¡/sub¿ Fuel Cell-Electric Propulsion on Aircraft Configuration and Integration*. [Online]. Available: https://arc.aiaa.org/doi/abs/10.2514/6.2021-2409

[16] M. H. Nehrir and C. Wang, *Dynamic Modeling and Simulation of PEM Fuel Cells*, 2009, pp. 57–84.